1   *In vivo* **imaging of cannabinoid type 2 receptors, functional and structural alterations in**

2   **mouse model of cerebral ischemia by PET and MRI**

3   Ruiqing Ni,[1,2] Adrienne Müller Herde,[3] Ahmed Haider,[3] Claudia Keller,[3] Georgios Louloudis,[1]

4   Markus Vaas,[1] Roger Schibli,[3] Simon M. Ametamey,[3] Jan Klohs,[1] Linjing Mu[3,4]*

5   [1]Institute for Biomedical Engineering, University of Zurich & ETH Zurich, Zurich, Switzerland

6   [2]Institute for Regenerative Medicine, University of Zurich, Zurich, Switzerland

7   [3]Department of Chemistry and Applied Biosciences, ETH Zurich, Zurich, Switzerland

8   [4]Department of Nuclear Medicine, University Hospital Zurich, Zurich, Switzerland

9

10

11   Corresponding author: Dr. Linjing Mu

12

13   **Author's details**

14   Dr. Linjing Mu

15   Department of Chemistry and Applied Biosciences, ETH Zurich, Zurich, Switzerland

16   Address: ETH Zürich, HCI E 388.1 Vladimir-Prelog-Weg 1-5/10 Zürich 8093

17   Email: linjing.mu@pharma.ethz.ch

18   Phone: +41 44 633 61 96

19

20

21

Abstract

Background and purpose: Brain ischemia is one of the most important pathologies of the central nervous system. Non-invasive molecular imaging methods have the potential to provide critical insights into the temporal dynamics and follow alterations of receptor expression and metabolism in ischemic stroke. The aim of this study was to assess the cannabinoid type 2 receptors (CB_2R) levels in transient middle cerebral artery occlusion (tMCAO) mouse models at subacute stage using positron emission tomography (PET) with our novel tracer [^{18}F]RoSMA-18-d6, and structural imaging by magnetic resonance imaging (MRI).

Methods: Our recently developed CB_2R PET tracer [^{18}F]RoSMA-18-d6 was used for imaging the neuroinflammation at 24 h after reperfusion in tMCAO mice. The RNA expression levels of CB_2R and other inflammatory markers were analyzed by quantitative real-time polymerase chain reaction using brain tissues from tMCAO (1 h occlusion) and sham-operated mice. [^{18}F]fluorodeoxyglucose (FDG) was included for evaluation of the cerebral metabolic rate of glucose (CMRglc). In addition, diffusion-weighted imaging and T_2-weighted imaging were performed for anatomical reference and delineating the lesion in tMCAO mice.

Results: mRNA expressions of inflammatory markers *TNF-α, Iba1, MMP9* and *GFAP, CNR2* were increased at 24 h after reperfusion in the ipsilateral compared to contralateral hemisphere of tMCAO mice, while mRNA expression of the neuronal marker *MAP-2* was markedly reduced. Reduced [^{18}F]FDG uptake was observed in the ischemic striatum of tMCAO mouse brain at 24 h after reperfusion. Although higher activity of [^{18}F]RoSMA-18-d6 in *ex-vivo* biodistribution studies and higher standard uptake value ratio (SUVR) were detected in the ischemic ipsilateral

43   compared to contralateral striatum in tMCAO mice, the *in-vivo* specificity of [^{18}F]RoSMA-18-d6

44   was confirmed only in the CB$_2$R-rich spleen.

45   Conclusions: This study revealed an increased [^{18}F]RoSMA-18-d6 measure of CB$_2$R and a

46   reduced [^{18}F]FDG measure of CMRglc in ischemic striatum of tMCAO mice at subacute stage.

47   [^{18}F]RoSMA-18-d6 might be a promising PET tracer for detecting CB$_2$R alterations in animal

48   models of neuroinflammation without neuronal loss.

49

50   **Key words:** cannabinoid type 2 receptor; [^{18}F]RoSMA-18-d6; ischemic stroke;

51   neuroinflammation; magnetic resonance imaging; positron emission tomography

52

Introduction

The pathophysiology of ischemic stroke is complex and associated with a myriad of cellular and molecular pathways. The severe reduction in cerebral blood flow (CBF) initiates a cascade of hemodynamic, vascular and inflammatory processes in a time-dependent manner in the supplied brain territory, and subsequent defensive response for repair related to lesion expansion and containment. Irreversible tissue damage occurs in the core of the ischemic area; while neurons in the ischemic penumbra face excitotoxicity, peri-infarct polarizations, inflammation and apoptosis, leading to a secondary tissue damage and expansion of the lesion if reperfusion cannot be restored within an early time frame [2-4]. Neuroinflammation post stroke has been an important therapeutic target. Anti-inflammatory, immunomodulatory treatments and microglia-targeted therapy were evaluated in clinical stroke trials [5-7]. Thus, there is a need for imaging the regional neuroinflammatory pattern for understanding disease mechanism and for therapeutic monitoring.

Positron emission tomography (PET) using [^{18}F]fluorodeoxyglucose ([^{18}F]FDG) for cerebral metabolic rate of glucose (CMRglc), [^{15}O]H$_2$O for perfusion imaging, and diffusion weighted (DW) magnetic resonance imaging (MRI) are valuable tools to support understanding of the pathophysiology in patients with ischemic stroke [3, 8-14]. However, *in vivo* imaging of neuroinflammation and gliosis is challenging [12, 13, 15]. One reason is that the astrocytes and microglia are highly dynamic and heterogeneous in their subtypes, locations and activation status. Additionally, the identification of an ideal target for neuroinflammation imaging is highly demanding. Translocator protein (TSPO) is the most widely used neuroinflammation target for PET imaging. [^{11}C]PK-11195, the first generation TSPO PET tracer, and several second-generation tracers such as [^{11}C]DAA1106, [^{11}C]PBR06, [^{11}C]PBR28, [^{11}C]GE180, and

4

76 [^{18}F]DPA-713, [^{18}F]DPA-714 [16-24] have been evaluated in (pre)-clinical studies. So far,

77 imaging neuroinflammation with TSPO PET tracers yielded controversial results in rodents and

78 patients with ischemic stroke [1, 13, 20]. Thus, the development of novel PET probes for

79 visualizing alternative targets in neuroinflammation have received great attention in recent years

80 [25-27].

81   Cannabinoid type 2 receptors (CB$_2$R) are mainly expressed by immune cells including

82 monocytes and macrophages. In the brain, CB$_2$Rs are primarily found on microglia and have low

83 expression levels under physiological conditions [2, 4, 28]. Upregulation of brain CB$_2$R

84 expression is reported under acute inflammation such as ischemic stroke, and related to lesion

85 extension in the penumbra and subsequent functional recovery [29]. Treatment with CB$_2$R

86 agonists has been shown to be neuroprotective and attenuates macrophage/microglial activation

87 in the mouse models of cerebral ischemia [29, 42-45]. CB$_2$R is also upregulated in other brain

88 diseases with involvement of inflammation/microglia under chronic inflammation in

89 neurodegenerative diseases such as Alzheimer's disease [30-33] and senescence-accelerated

90 models [34], associated with amyloid-β deposits[28, 35-41].

91   Several structural scaffolds of CB$_2$R PET tracers have recently been developed [46-50]

92 including pyridine derivatives, oxoquinoline derivatives; thiazole derivatives [51, 52];

93 oxadiazole derivatives [53]; carbazole derivatives [54]; imidazole derivative [55]; and thiophene

94 derivatives [56, 57]. In this study, our newly developed pyridine derivative [^{18}F]RoSMA-18-d6,

95 which exhibited sub-nanomolar affinity and high selectivity towards CB2R (Ki: 0.8 nM,

96 CB2R/CB1R > 12'000) [58] is selected as the CB$_2$R PET tracer.

97   The aim of the current study was to evaluate the novel CB$_2$R tracer [^{18}F]RoSMA-18-d6 in

98 the transient middle cerebral artery occlusion (tMCAO) mouse models of focal cerebral ischemia

99   [60-66] using microPET. In addition, [^{18}F]FDG was included for evaluation of the cerebral

100   metabolic rate of glucose (CMRglc). Diffusion-weighted imaging and T$_2$- weighted imaging

101   were performed for anatomical reference and for delineating the lesion in tMCAO mice.

102

103   **Methods**

104   Radiosynthesis

105   [^{18}F]RoSMA-18-d6 was synthesized by nucleophilic substitution of the tosylate precursor with

106   [^{18}F]KF/Kryptofix222 in acetonitrile [58]. The crude product was purified by reverse phase

107   semi-preparative high-performance liquid chromatography and formulated with 5 % ethanol in

108   water for intravenous injection and for biological evaluations. In a typical experiment, a

109   moderate radiochemical yield of ~ 12 % (decay corrected) was achieved with a radiochemical

110   purity > 99 %. The molar activities ranged from 156 to 194 GBq/μmol at the end of synthesis.

111   The identity of the final product was confirmed by comparison with the HPLC retention time of

112   the non-radioactive reference compound by co-injection. [^{18}F]FDG was obtained from a routine

113   clinical production from the University Hospital Zurich, Switzerland.

114

115   Animals

116   Twenty-four male C57BL/6J mice were obtained from Janvier Labs (Le Genest-Saint-Isle,

117   France). The mice were scanned at 8–10 weeks of age (20–25 g body weight). Mice were

118   randomly allocated to sham-operation (n = 10) or tMCAO (n = 14). Mice underwent MRI,

119   μPET/ computed tomography (CT), and 2,3,5-Triphenyltetrazolium chloride (TTC) histology

120   staining for validation 24 h or 48 h after reperfusion. Animals were housed in ventilated cages

121   inside a temperature-controlled room, under a 12-hour dark/light cycle. Pelleted food

122   (3437PXL15, CARGILL) and water were provided *ad-libitum.* Paper tissue and red Tecniplast

123   mouse house® (Tecniplast, Milan, Italy) shelters were placed in cages as environmental

124   enrichments. All experiments were performed in accordance with the Swiss Federal Act on

125   Animal Protection and were approved by the Cantonal Veterinary Office Zurich (permit number:

126   ZH018/14 and ZH264/16).

127

128   Surgeries for tMCAO and sham-operation were performed using standard-operating procedures

129   as described before [67, 68]. Anaesthesia was initiated by using 3 % isoflurane (Abbott, Cham,

130   Switzerland) in a 1:4 oxygen/air mixture, and maintained at 2 %. Before the surgical procedure, a

131   local analgesic (Lidocaine, 0.5 %, 7 mg/kg, Sintectica S.A., Switzerland) was administered

132   subcutaneously (s.c.). Temperature was kept constant at 36.5 ± 0.5 °C with a feedback controlled

133   warming pad system. All surgical procedures were performed in 15-30 min. After surgery,

134   buprenorphine was administered as s.c. injection (Temgesic, 0.1 mg/kg b.w.), and at 4 h after

135   reperfusion and supplied thereafter via drinking water (1 mL/32 mL of drinking water) until 24 h

136   or 48 h. Animals received softened chow in a weighing boat on the cage floor to encourage

137   eating. tMCAO animals were excluded from the study if they met one of the following criteria:

138   Bederson testing was performed 2h post-reperfusion. Bederson score of 0, no reflow after

139   filament removal, and premature death.

140

141   *mRNA isolation, reverse-transcription reaction and real-time polymerase chain reaction*

142   Brain hemispheres of C57BL/6 mouse, tMCAO mice at 24 h and 48 h post reperfusion were

143   used for total mRNA isolation according to the protocols of the Isol-RNA Lysis Reagent (5

144   PRIME, Gaithersburg, USA) and the bead-milling TissueLyser system (Qiagen, Hilden,

145   Germany). QuantiTect® Reverse Transcription Kit (Qiagen, Hilden, Germany) was used to

146   generate cDNA. The primers (Microsynth, Balgach, Switzerland) used for the quantitative

147   polymerase chain reaction (qPCR) are summarized in **Supplementary Table 1**. Quantitation of

148   *CNR2, Iba1, TNF-α, MMP9, GFAP* and *MAP-2* mRNA expression was performed with the

149   DyNAmo™ Flash SYBR® Green qPCR Kit (Thermo Scientific, Runcorn, UK) using a 7900 HT

150   Fast Real-Time PCR System (Applied Biosystems, Carlsbad, USA). The amplification signals

151   were detected in real-time, which permitted accurate quantification of the amounts of the initial

152   RNA template during 40 cycles according to the manufacturer's protocol. All reactions were

153   performed in duplicates and in two independent runs. Quantitative analysis was performed using

154   the SDS Software (v2.4) and a previously described $2-\Delta\Delta Ct$ quantification method [69]. The

155   specificity of the PCR products of each run was determined and verified with the SDS

156   dissociation curve analysis feature.

157

158   *In vivo* MRI

159   Data were acquired at 24 h after reperfusion on a 7 T Bruker Pharmascan (Bruker BioSpin

160   GmbH, Germany), equipped with a volume resonator operating in quadrature mode for

161   excitation and a four element phased-array surface coil for signal reception and operated by

162   Paravision 6.0 (Bruker BioSpin) [67, 70-72]. Mice were anesthetized with an initial dose of 4 %

163   isoflurane in oxygen/air (200:800 ml/min) and maintained at 1.5 % isoflurane in oxygen/air

164   (100:400 ml/min). Body temperature was monitored with a rectal temperature probe (MLT415,

165   ADInstruments) and kept at 36.5 °C ± 0.5 °C using a warm water circuit integrated into the

166   animal support (Bruker BioSpin GmbH, Germany). T_2-weighted MR images were obtained

167   using a spin echo sequence (TurboRARE) with an echo time 3 ms, repetition time 6 ms, 100

168   averages, slice thickness 1 mm, field-of-view 2.56 cm × 1.28 cm, matrix size 256 × 128, giving

169   an in-plane resolution of 100 μm × 100 μm. For DWI, a four-shot spin echo–echo planar imaging

170   sequence with an echo time = 28 ms, repetition time = 3000 [70, 71] acquired with a field-of-

171   view of 3.3 cm × 2 cm and a matrix size of 128 × 128, resulting in a nominal voxel size of 258

172   μm × 156 μm. Diffusion-encoding was applied in the x-, y-, and z-directions with b-values of

173   100, 200, 400, 600, 800, and 1000 s/mm^2, respectively, acquisition time 3 min 48 s. The

174   ischemic lesion was determined as an area of significant reduction of the apparent diffusion

175   coefficient (ADC) value compared with the unaffected contralateral side [73]. On T_2-weighted

176   images, the lesion was determined as an area of hyperintensities compared with the contralateral

177   side.

178

179   *In vivo* microPET studies

180   MicroPET/CT scans were performed at 24 h after reperfusion with a calibrated SuperArgus

181   μPET/CT scanner (Sedecal, Madrid, Spain) with an axial field-of-view of 4.8 cm and a spatial

182   resolution of 1.6–1.7 mm (full width at half maximum). tMCAO and the sham-operated

183   C57BL/6J mice were anesthetized with ca. 2.5 % isoflurane in oxygen/air (1:1) during tracer

184   injection and the whole scan time period. The formulated radioligand solution ([^{18}F]FDG: 9.9-11

185   MBq or [^{18}F]RoSMA-18-d6: 7.2-13 MBq) was administered via tail vein injection, and mice

186   were dynamically scanned for 60 min. For blocking experiments, 1.5 mg/kg GW405833 was

187   dissolved in a vehicle of 2 % Cremophor (v/v), 10 % ethanol (v/v), and 88 % water for injection

188   (v/v) and injected together with [^{18}F]RoSMA-18-d6. Body temperature was monitored by a

189   rectal probe and kept at 37 °C by a heated air stream (37 °C). The anesthesia depth was measured

190   by the respiratory frequency (SA Instruments, Inc., Stony Brook, USA). μPET acquisitions were

191 combined with CT for anatomical orientation and attenuation correction. The obtained data were

192 reconstructed in user-defined time frames with a voxel size of $0.3875 \times 0.3875 \times 0.775$ mm^3 as

193 previously described [74].

194

195 Triphenyltetrazolium chloride (TTC) staining

196 To assess the ischemic lesion severity in the brain of tMCAO mice and to validate the absence of

197 lesion in the sham-operated mice, staining with TTC staining was performed. After

198 measurements mice were euthanized, their brains were removed and 1-mm thick brain slices

199 were obtained with a brain matrix. Slices were incubated in a 2.5 % TTC solution (Sigma-

200 Aldrich, Switzerland) in PBS at 37 °C for 3 min. Photographs of the brain sections were taken.

201 Edema-corrected lesion volumes were quantified as described [75].

202

203 Biodistribution studies in the mouse brain

204 After PET/CT scanning of tMCAO mice at 24 h after reperfusion with [^{18}F]RoSMA-18-d6,

205 animals were sacrificed at 70 min post injection by decapitation. The spleen and brain regions of

206 ischemic ipsilateral area and contralateral hemisphere were collected for analysis with a gamma

207 counter. The accumulated radioactivities in the different tissues were expressed as percent

208 normalized injected dose per gram of tissue normalized to 20 g body weight of the animals

209 (norm. percentage injected dose per gram tissue (% ID/g tissue)).

210

211 Data analysis and Statistics

212 Images were processed and analyzed using PMOD 4.2 software (PMOD Technologies Ltd.,

213 Zurich, Switzerland). The time–activity curves were deduced from specific volume-of-interest

214   that were defined based on a mouse MRI T_2-weighted image template [76]. Radioactivity is

215   presented as standardized uptake value (SUV) (decay-corrected radioactivity per cm^3 divided by

216   the injected dose per gram body weight). [^{18}F]RoSMA-18-d6 SUVR was calculated by using the

217   midbrain in the corresponding hemisphere as reference brain region. For [^{18}F]FDG PET, regional

218   SUV was calculated. Two-way ANOVA with Sidak post-hoc analysis was used for comparison

219   between groups (Graphpad Prism 9.0, CA, U.S.A).

220

221   **Results**

222   Increased expression of inflammation makers and neuronal damage after focal cerebral ischemia

223   in tMCAO mice

224   mRNA levels were measured to address the question whether mouse non-ischemic and ischemic

225   hemispheres differ in their expression levels of *CNR2* and other inflammatory genes. *CNR2*

226   mRNA expression was increased to around 1.3 fold after 24 h reperfusion and at 48 h in the

227   ipsilateral comparing to contralateral hemisphere (**Fig. 1a**). Similar 1.5-2.5 fold increases were

228   observed in the mRNA expression of inflammatory markers including *TNF-α, Iba1, MMP9* and

229   *GFAP* at 24 h and 48 h after reperfusion in the ipsilateral compared to contralateral brain region

230   (**Fig. 1b-e**). *MAP-2* expression has been shown to be a reliable marker of neurons that undergo

231   irreversible cell death [77, 78]. The neuron-specific *MAP-2* expression was markedly reduced in

232   the ipsilateral compared to contralateral hemisphere at 24 h and 48 h after reperfusion (**Fig. 1f**).

233   As similar *CNR2* mRNA expression were observed in 24 h and 48 h, our studies were performed

234   at early time point of 24 h after reperfusion for investigating the functional, structural and

235   molecular changes in the following experiments.

236

237 Reduced cerebral glucose metabolism and structural MRI lesion following tMCAO

238 Reduced [^{18}F]FDG uptake was observed in the presumed MCA territory of the ipsilateral

239 hemisphere in tMCAO mice, while there was no difference in [^{18}F]FDG uptake between

240 hemispheres in sham-operated mice (**Fig. 2a**). SUVs were significantly lower in the ipsilateral in

241 the striatum in tMCAO compared to the contralateral side and compared to the same region in

242 sham-operated mice 1.8 vs 1.4 (**Fig. 2b**). There were no differences in [^{18}F]FDG uptake in the

243 cortex and cerebellum between the ipsilateral and contralateral hemisphere in tMCAO mice and

244 sham-operated mice. T_2-weighted MRI and DWI imaging were performed in tMCAO and sham-

245 operated animals at 24 h after reperfusion (**Fig. 2c**). The lesions in the ipsilateral side in the

246 striatum and cortex were visible as areas of decreased values on the ADC maps calculated from

247 DWI, and as areas of increased intensities on the T_2-weighted MR images at 24 h after

248 reperfusion following 1 h tMCAO (**Figs. 2c-d**). Ischemic lesions in the tMCAO were also seen

249 *ex vivo* as white areas while viable tissue appeared red in TTC stained brain sections(**Fig. 2e**).

250 Homogenous deep red color was observed across both hemispheres in sham-operated mice,

251 verifying the absence of any lesion. The hemispheric lesion volumes in tMCAO mice were 42.8

252 ± 10.2 % (mean ± standard deviation).

253

254 Increased [^{18}F]RoSMA-18-d6 retention in the striatum after tMCAO

255 To analyze the distribution of [^{18}F]RoSMA-18-d6 in tMCAO mice brain, dynamic µPET/CT

256 scans were performed at 24 h after reperfusion. The standard uptake values (SUVs) of

257 [^{18}F]RoSMA-18-d6 did not reveal significant difference in various brain regions of tMCAO mice

258 (**Supplementary Fig 1**). However, we found a reduced uptake at early time frame (1-3 min) and

259   a similar uptake after 7 min in the ipsilateral side compared to that of contralateral side (Fig. 3a).

260   Thus, to exclude the perfusion influence, we averaged the brain signals from 21-61 min and

261   selected the midbrain as the reference region. Higher [^{18}F]RoSMA-18-d6 SUVR was observed in

262   the ischemic ipsilateral striatum compared to the contralateral striatum (two-way ANOVA with

263   Sidak multiple comparison correction, 0.97 ± 0.02 vs 0.87 ± 0.06, p = 0.0274), but not in other

264   brain regions such as cortex (**Fig. 3b, c**). The increased signals at ischemic ipsilateral striatum,

265   however, could not be blocked by the selective CB$_2$R agonist GW405833 (**Fig. 3c**).

266

267   At the end of the *in vivo* experiments, we dissected the mice to verify the activity accumulation

268   and specificity of [^{18}F]RoSMA-18-d6 in the spleen and different brain regions with a gamma

269   counter. In line with the results obtained from the averaged SUVRs in the tMCAO mouse brain,

270   the radioactivity in the ipsilateral side was indeed significant higher than that of the contralateral

271   hemisphere (0.037 ± 0.007 vs 0.026 ± 0.003, n = 5 each group), but no blockade effect was seen

272   under blocking conditions (**Fig. 4a**). As expected, radioactivity in the CB$_2$R-rich spleen was

273   much higher than the brain and 58 % of the signals was blocked by co-injection of CB$_2$R specific

274   ligand GW405833, demonstrating specific target engagement of [^{18}F]RoSMA-18-d6 *in vivo* (**Fig.**

275   **4b**).

276

277   **Discussion**

278   This study assessed the utility of CB$_2$R PET tracer [^{18}F]RoSMA-18-d6 for imaging

279   tMCAO mouse at subacute stage, concomitant with decreased CMRglc levels and formation of a

280   structural lesion. Previous PET imaging of stroke animal models led to inconclusive results. In a

281   rat model of photothrombotic stroke at 24 h after surgery, increased [^{11}C]NE40 (CB$_2$R tracer)

13

282   uptake and unvaried [^{11}C]PK11195 (TSPO tracer) uptake were reported [79]. In another study,

283   [^{11}C]NE40 uptake did not show any difference in the same rat model of photothrombotic stroke

284   [80]. Moreover, reduced [^{11}C]A836339 (CB$_2$R tracer) uptake was reported in a focal tMCAO rat

285   model over 1-28 days after occlusion [51]. Possible reasons for these different observations

286   include the time point of assessment, different methods for inducing acute stroke (transient or

287   permanent ischemia) resulting in variations of ischemic severity and levels of inflammatory-cell

288   expression [43].

289   CB$_2$R has negligible expression in the mouse brain and is mainly expressed in the spleen

290   under physiological conditions [30, 36, 60-65, 81]. Under neuroinflammatory conditions, CB$_2$R

291   is upregulated in activated microglial cells. In this study, we used quantitative real-time

292   polymerase chain reaction to measure gene expression levels of *CNR2, TNF-α, Iba1, MMP9,*

293   *GFAP* and *MAP-2* at 24 h and 48 h. All tested inflammatory markers displayed increased mRNA

294   levels in the ipsilateral brain hemisphere, in agreement with the reported findings in tMCAO

295   mouse model [29, 45, 82, 83]. In line with the increased *CNR2* gene expression levels,

296   significantly higher [^{18}F]RoSMA-18-d6 SUVR (standard uptake value ratio) was observed in

297   striatum at ipsilateral vs contralateral under baseline conditions in our PET studies. The 50 %

298   reduction of the neuronal marker *MAP-2* indicated neuronal damage.

299   The dynamic μPET scan using [^{18}F]RoSMA-18-d6 indicated a reduced perfusion in the

300   lesion brain regions at the first time frame of 1-3 minutes. This is probably due to the changes of

301   microvascular response (no-reflow phenomenon) and the reduction in neuronal activity. Taking

302   the midbrain as the reference region, the ratios of SUV averaged from 21-61 min revealed

303   increased [^{18}F]RoSMA-18-d6 SUVR in the ipsilateral ischemic striatum compared to that of the

304   contralateral side. Our *ex vivo* bio-distribution studies confirmed the difference of the

14

305 radioactivity distribution in the left and right brain hemisphere. The *in vivo* specificity of

306 [^{18}F]RoSMA-18-d6 towards CB$_2$R is evidenced by a 58 % reduction in radioactivity in the

307 mouse spleen under blockade conditions in *ex vivo* biodistribution studies. Underlying reasons

308 for the lack of specificity of [^{18}F]RoSMA-18-d6 in the mouse brain may because 1) the increased

309 tracer availability in the blood induced by blocking the CB$_2$R peripheral targets in the presence

310 of the blocker GW405833; and 2) the relatively low brain uptake of our CB$_2$R-selective

311 radioligand [^{18}F]RoSMA-18-d6 in the mouse brain resulted in undetectable changes of

312 radiosignals under baseline and blockade conditions. Notably, the time-activity curves of

313 [^{18}F]RoSMA-18-d6 in tMCAO mouse brain showed remarkably higher initial brain uptake under

314 blockade conditions than the baseline in both sides of the mouse brain (**Supplementary Fig 1**),

315 indicating the influence of blocking CB$_2$R target in the peripheral organs on the availability of

316 radiotracer concentrations in the blood. In our previous studies with Wistar rat, the spleen uptake

317 of [^{18}F]RoSMA-18-d6 was blocked by nearly 90 % suggesting a high possibility of species

318 difference of [^{18}F]RoSMA-18-d6 binding [57]. Therefore, we speculate that rat stroke models

319 might be superior to mice models for imaging neuroinflammation with CB$_2$R PET tracers.

320   We observed that [^{18}F]FDG measure of CMRglc was reduced in the ischemic areas i.e.

321 ipsilateral striatum of the tMCAO mice at 24 h after reperfusion. The reduced CMRglc was

322 reported in many earlier studies in disease animal models and in stroke patients [84-87], masking

323 CMRglc reduction of neuronal tissue in the brain At an extended time points of the recovery

324 stage from day 4 - 40, an increased CMRglc level was reported in the ischemic regions due to the

325 increased consumption from inflammatory cells along with microglial activation [88-90].

326   There are several limitations in the current study. 1) As there is no reliable specific CB$_2$R

327 antibody, we did not include immunohistochemical staining for CB$_2$R protein distribution in the

15

328   mouse brain. The qPCR measures of *CNR2* mRNA level provided an alternative readout, but do

329   not provide spatial distribution of cerebral CB_2R expression. 2) Due to the logistic barrier, MRI

330   and μPET/CT scans were performed with different cohorts of animals. Nevertheless, standard

331   operating procedures for the surgery were used. 3) Our *in vivo* data with tMCAO mice were

332   collected at 24 h after surgery, longitudinal imaging of tMCAO mice with [^{18}F]RoSMA-18-d6

333   along with structural and functional readout will provide further insight into the spatial-temporal

334   dynamics of CB_2R expression in the brain.

335

Conclusion

337   Our newly developed CB_2R PET tracer [^{18}F]RoSMA-18-d6 revealed limited utility to image

338   neuroinflammation in the ischemic ipsilateral of the tMCAO mice at 24 h after reperfusion.

339   Although lesion regions in tMCAO mouse brain could be followed by the ratios of averaged

340   SUVs from 21-61 with midbrain as the reference region, the in-vivo specificity of [^{18}F]RoSMA-

341   18-d6 was confirmed only in the CB2R-rich spleen. Different neuroinflammatory animal models

342   which has comparable neuronal numbers in the lesion regions are recommended for evaluation

343   of CB_2R in further PET imaging studies.

344

Appendix

Acknowledgements

16

351

Funding

357

Abbreviations

359 ADC: Apparent diffusion coefficient; CB_2R: Cannabinoid type 2 receptors; CBF: Cerebral blood

360 flow; CMRglc: Cerebral metabolic rate of glucose; CT: computed tomography; DW: Diffusion

361 weighted; FDG: fluorodeoxyglucose; % ID/g tissue: Injected dose per gram tissue; MRI:

362 Magnetic resonance imaging; PET: Positron emission tomography: SUV: Standardized uptake

363 value; SUVR: Standard uptake value ratio; tMCAO: transient middle cerebral artery occlusion;

364 TSPO: Translocator protein; TTC: Triphenyltetrazolium chloride.

365

Availability of data and materials

367 The data used and analyzed in the current study are available from the corresponding authors

368 upon request.

369

Ethics approval and consent to participate

371   All experiments were performed in accordance with the Swiss Federal Act on Animal Protection

372   and were approved by the Cantonal Veterinary Office Zurich (permit number: ZH018/14 and

373   ZH264/16).

374

375   **Competing interests**

376   The authors declare no conflicts of interest.

377

378   **Consent for publication**

379   Not applicable.

380

381   **Authors' contribution**

382   RN, JK, LM, SMA designed the study; RN, KC, AH, AMH, GL, LM performed the experiment,

383   RN, LM performed data analysis, RN, JK, LM wrote the initial manuscript. All authors read and

384   approved the final manuscript.

References

385

386 1.   Kreisl WC, Kim MJ, Coughlin JM, Henter ID, Owen DR, Innis RB: **PET imaging of**
387   **neuroinflammation in neurological disorders.** *Lancet Neurol* 2020, **19:**940-950.
388 2.   Astrup J: **Energy-requiring cell functions in the ischemic brain. Their critical supply**
389   **and possible inhibition in protective therapy.** *J Neurosurg* 1982, **56:**482-497.
390 3.   Heiss W-D: **Ischemic Penumbra: Evidence From Functional Imaging in Man.**
391   *Journal of Cerebral Blood Flow & Metabolism* 2000, **20:**1276-1293.
392 4.   Dirnagl U, Iadecola C, Moskowitz MA: **Pathobiology of ischaemic stroke: an**
393   **integrated view.** *Trends Neurosci* 1999, **22:**391-397.
394 5.   Dabrowska S, Andrzejewska A, Lukomska B, Janowski M: **Neuroinflammation as a**
395   **target for treatment of stroke using mesenchymal stem cells and extracellular**
396   **vesicles.** *Journal of Neuroinflammation* 2019, **16:**178.
397 6.   Anrather J, Iadecola C: **Inflammation and Stroke: An Overview.** *Neurotherapeutics*
398   2016, **13:**661-670.
399 7.   Lambertsen KL, Finsen B, Clausen BH: **Post-stroke inflammation—target or tool for**
400   **therapy?** *Acta Neuropathol* 2019, **137:**693-714.
401 8.   Evans NR, Tarkin JM, Buscombe JR, Markus HS, Rudd JHF, Warburton EA: **PET**
402   **imaging of the neurovascular interface in cerebrovascular disease.** *Nature Reviews*
403   *Neurology* 2017, **13:**676-688.
404 9.   Marchal G, Rioux P, Petit-Tabou MC, Derlon JM, Baron JC, Serrati C, Viader F, de la
405   Sayette V, Le Doze F, Lochon P, et al: **PET imaging of cerebral perfusion and oxygen**
406   **consumption in acute ischaemic stroke: relation to outcome.** *The Lancet* 1993,
407   **341:**925-927.
408 10.   Muir KW, Buchan A, von Kummer R, Rother J, Baron J-C: **Imaging of acute stroke.**
409   *The Lancet Neurology* 2006, **5:**755-768.
410 11.   Carter SF, Herholz K, Rosa-Neto P, Pellerin L, Nordberg A, Zimmer ER: **Astrocyte**
411   **Biomarkers in Alzheimer's Disease.** *Trends Mol Med* 2019, **25:**77-95.
412 12.   Jain P, Chaney AM, Carlson ML, Jackson IM, Rao A, James ML: **Neuroinflammation**
413   **PET Imaging: Current Opinion and Future Directions.** *Journal of Nuclear Medicine*
414   2020, **61:**1107-1112.
415 13.   Zinnhardt B, Wiesmann M, Honold L, Barca C, Schafers M, Kiliaan AJ, Jacobs AH: **In**
416   **vivo imaging biomarkers of neuroinflammation in the development and assessment**
417   **of stroke therapies - towards clinical translation.** *Theranostics* 2018, **8:**2603-2620.
418 14.   Martín A, Macé E, Boisgard R, Montaldo G, Thézé B, Tanter M, Tavitian B: **Imaging of**
419   **Perfusion, Angiogenesis, and Tissue Elasticity after Stroke.** *Journal of Cerebral*
420   *Blood Flow & Metabolism* 2012, **32:**1496-1507.
421 15.   Venneti S, Lopresti BJ, Wiley CA: **Molecular imaging of microglia/macrophages in**
422   **the brain.** *Glia* 2013, **61:**10-23.
423 16.   Thiel A, Heiss WD: **Imaging of microglia activation in stroke.** *Stroke* 2011, **42:**507-
424   512.
425 17.   Boutin H, Murray K, Pradillo J, Maroy R, Smigova A, Gerhard A, Jones PA, Trigg W:
426   **18F-GE-180: a novel TSPO radiotracer compared to 11C-R-PK11195 in a**
427   **preclinical model of stroke.** *Eur J Nucl Med Mol Imag* 2015, **42:**503-511.

18. Lartey FM, Ahn GO, Shen B, Cord K-T, Smith T, Chua JY, Rosenblum S, Liu H, James ML, Chernikova S, et al: **PET Imaging of Stroke-Induced Neuroinflammation in Mice Using [18F]PBR06.** *Molecular Imaging and Biology* 2014, **16:**109-117.

19. Tóth M, Little P, Arnberg F, Häggkvist J, Mulder J, Halldin C, Gulyás B, Holmin S: **Acute neuroinflammation in a clinically relevant focal cortical ischemic stroke model in rat: longitudinal positron emission tomography and immunofluorescent tracking.** *Brain Structure and Function* 2016, **221:**1279-1290.

20. Chaney A, Cropper HC, Johnson EM, Lechtenberg KJ, Peterson TC, Stevens MY, Buckwalter MS, James ML: **11C-DPA-713 versus 18F-GE-180: A preclinical comparison of TSPO-PET tracers to visualize acute and chronic neuroinflammation in a mouse model of ischemic stroke.** *Journal of Nuclear Medicine* 2018**:**jnumed.118.209155.

21. Martín A, Boisgard R, Thézé B, Van Camp N, Kuhnast B, Damont A, Kassiou M, Dollé F, Tavitian B: **Evaluation of the PBR/TSPO Radioligand [18F]DPA-714 in a Rat Model of Focal Cerebral Ischemia.** *Journal of Cerebral Blood Flow & Metabolism* 2009, **30:**230-241.

22. Thiel A, Radlinska BA, Paquette C, Sidel M, Soucy J-P, Schirrmacher R, Minuk J: **The Temporal Dynamics of Poststroke Neuroinflammation: A Longitudinal Diffusion Tensor Imaging–Guided PET Study with ^{11}C-PK11195 in Acute Subcortical Stroke.** *Journal of Nuclear Medicine* 2010, **51:**1404-1412.

23. Zinnhardt B, Viel T, Wachsmuth L, Vrachimis A, Wagner S, Breyholz H-J, Faust A, Hermann S, Kopka K, Faber C, et al: **Multimodal Imaging Reveals Temporal and Spatial Microglia and Matrix Metalloproteinase Activity after Experimental Stroke.** *Journal of Cerebral Blood Flow & Metabolism* 2015, **35:**1711-1721.

24. Ishikawa A, Tokunaga M, Maeda J, Minamihisamatsu T, Shimojo M, Takuwa H, Ono M, Ni R, Hirano S, Kuwabara S, et al: **In Vivo Visualization of Tau Accumulation, Microglial Activation, and Brain Atrophy in a Mouse Model of Tauopathy rTg4510.** *J Alzheimers Dis* 2018, **61:**1037-1052.

25. Razansky D, Klohs J, Ni R: **Multi-scale optoacoustic molecular imaging of brain diseases.** *Eur J Nucl Med Mol Imaging* 2021.

26. Ling X, Zhang S, Shao P, Li W, Yang L, Ding Y, Xu C, Stella N, Bai M: **A novel near-infrared fluorescence imaging probe that preferentially binds to cannabinoid receptors CB2R over CB1R.** *Biomaterials* 2015, **57:**169-178.

27. Sarott RC, Westphal MV, Pfaff P, Korn C, Sykes DA, Gazzi T, Brennecke B, Atz K, Weise M, Mostinski Y, et al: **Development of High-Specificity Fluorescent Probes to Enable Cannabinoid Type 2 Receptor Studies in Living Cells.** *Journal of the American Chemical Society* 2020, **142:**16953-16964.

28. Stempel AV, Stumpf A, Zhang HY, Ozdogan T, Pannasch U, Theis AK, Otte DM, Wojtalla A, Racz I, Ponomarenko A, et al: **Cannabinoid Type 2 Receptors Mediate a Cell Type-Specific Plasticity in the Hippocampus.** *Neuron* 2016, **90:**795-809.

29. Zarruk JG, Fernandez-Lopez D, Garcia-Yebenes I, Garcia-Gutierrez MS, Vivancos J, Nombela F, Torres M, Burguete MC, Manzanares J, Lizasoain I, Moro MA: **Cannabinoid type 2 receptor activation downregulates stroke-induced classic and alternative brain macrophage/microglial activation concomitant to neuroprotection.** *Stroke* 2012, **43:**211-219.

30. López A, Aparicio N, Pazos MR, Grande MT, Barreda-Manso MA, Benito-Cuesta I, Vázquez C, Amores M, Ruiz-Pérez G, García-García E, et al: **Cannabinoid CB2 receptors in the mouse brain: relevance for Alzheimer's disease.** *Journal of Neuroinflammation* 2018, **15:**158.

31. Rodriguez-Vieitez E, Ni R, Gulyas B, Toth M, Haggkvist J, Halldin C, Voytenko L, Marutle A, Nordberg A: **Astrocytosis precedes amyloid plaque deposition in Alzheimer APPswe transgenic mouse brain: a correlative positron emission tomography and in vitro imaging study.** *Eur J Nucl Med Mol Imaging* 2015, **42:**1119-1132

32. Heneka MT, Carson MJ, El Khoury J, Landreth GE, Brosseron F, Feinstein DL, Jacobs AH, Wyss-Coray T, Vitorica J, Ransohoff RM, et al: **Neuroinflammation in Alzheimer's disease.** *Lancet Neurol* 2015, **14:**388-405.

33. Rapic S, Backes H, Viel T, Kummer MP, Monfared P, Neumaier B, Vollmar S, Hoehn M, Van der Linden A, Heneka MT, Jacobs AH: **Imaging microglial activation and glucose consumption in a mouse model of Alzheimer's disease.** *Neurobiol Aging* 2013, **34:**351-354.

34. Yamagishi S, Iga Y, Nakamura M, Takizawa C, Fukumoto D, Kakiuchi T, Nishiyama S, Ohba H, Tsukada H, Sato K, Ouchi Y: **Upregulation of cannabinoid receptor type 2, but not TSPO, in senescence-accelerated neuroinflammation in mice: a positron emission tomography study.** *Journal of Neuroinflammation* 2019, **16:**208.

35. Di Marzo V, Stella N, Zimmer A: **Endocannabinoid signalling and the deteriorating brain.** *Nat Rev Neurosci* 2015, **16:**30-42.

36. Van Sickle MD, Duncan M, Kingsley PJ, Mouihate A, Urbani P, Mackie K, Stella N, Makriyannis A, Piomelli D, Davison JS, et al: **Identification and functional characterization of brainstem cannabinoid CB2 receptors.** *Science* 2005, **310:**329-332.

37. Xi ZX, Peng XQ, Li X, Song R, Zhang HY, Liu QR, Yang HJ, Bi GH, Li J, Gardner EL: **Brain cannabinoid CB(2) receptors modulate cocaine's actions in mice.** *Nat Neurosci* 2011, **14:**1160-1166.

38. Benito C, Tolón RM, Pazos MR: **Cannabinoid CB2 receptors in human brain inflammation.** *Br J Pharmacol* 2008, **153**.

39. Koppel J, Vingtdeux V, Marambaud P, D'Abramo C, Jimenez H, Stauber M, Friedman R, Davies P: *CB2 Receptor Deficiency Increases Amyloid Pathology and Alters Tau Processing in a Transgenic Mouse Model of Alzheimer's Disease.* 2014.

40. Aso E, Ferrer I: **CB2 Cannabinoid Receptor As Potential Target against Alzheimer's Disease.** *Frontiers in Neuroscience* 2016, **10**.

41. Parbo P, Ismail R, Hansen KV, Amidi A, Marup FH, Gottrup H, Braendgaard H, Eriksson BO, Eskildsen SF, Lund TE, et al: **Brain inflammation accompanies amyloid in the majority of mild cognitive impairment cases due to Alzheimer's disease.** *Brain* 2017, **140:**2002-2011.

42. Ronca RD, Myers AM, Ganea D, Tuma RF, Walker EA, Ward SJ: **A selective cannabinoid CB2 agonist attenuates damage and improves memory retention following stroke in mice.** *Life Sci* 2015, **138:**72-77.

43. Bravo-Ferrer I, Cuartero MI, Zarruk JG, Pradillo JM, Hurtado O, Romera VG, Diaz-Alonso J, Garcia-Segura JM, Guzman M, Lizasoain I, et al: **Cannabinoid Type-2**

518   **Receptor Drives Neurogenesis and Improves Functional Outcome After Stroke.**
519   *Stroke* 2017, **48:**204-212.
520   44. Zhang M, Martin BR, Adler MW, Razdan RK, Jallo JI, Tuma RF: **Cannabinoid CB(2)**
521   **receptor activation decreases cerebral infarction in a mouse focal**
522   **ischemia/reperfusion model.** *J Cereb Blood Flow Metab* 2007, **27:**1387-1396.
523   45. Yu SJ, Reiner D, Shen H, Wu KJ, Liu QR, Wang Y: **Time-Dependent Protection of**
524   **CB2 Receptor Agonist in Stroke.** *PLoS One* 2015, **10:**e0132487.
525   46. Spinelli F, Capparelli E, Abate C, Colabufo NA, Contino M: **Perspectives of**
526   **Cannabinoid Type 2 Receptor (CB2R) Ligands in Neurodegenerative Disorders:**
527   **Structure-Affinity Relationship (SAfiR) and Structure-Activity Relationship (SAR)**
528   **Studies.** *J Med Chem* 2017.
529   47. Ni R, Mu L, Ametamey S: **Positron emission tomography of type 2 cannabinoid**
530   **receptors for detecting inflammation in the central nervous system.** *Acta Pharmacol*
531   *Sin* 2019, **40:**351-357.
532   48. Spinelli F, Mu L, Ametamey SM: **Radioligands for positron emission tomography**
533   **imaging of cannabinoid type 2 receptor.** *J Labelled Comp Radiopharm* 2018, **61:**299-
534   308.
535   49. Hou L, Rong J, Haider A, Ogasawara D, Varlow C, Schafroth MA, Mu L, Gan J, Xu H,
536   Fowler CJ, et al: **Positron Emission Tomography Imaging of the Endocannabinoid**
537   **System: Opportunities and Challenges in Radiotracer Development.** *Journal of*
538   *Medicinal Chemistry* 2021, **64:**123-149.
539   50. Varlow C, Boileau I, Wey HY, Liang SH, Vasdev N: **Classics in Neuroimaging:**
540   **Imaging the Endocannabinoid Pathway with PET.** *ACS Chem Neurosci* 2020,
541   **11:**1855-1862.
542   51. Pottier G, Gomez-Vallejo V, Padro D, Boisgard R, Dolle F, Llop J, Winkeler A, Martin
543   A: **PET imaging of cannabinoid type 2 receptors with [11C]A-836339 did not**
544   **evidence changes following neuroinflammation in rats.** *J Cereb Blood Flow Metab*
545   2017, **37:**1163-1178.
546   52. Moldovan R-P, Deuther-Conrad W, Teodoro R, Wang Y, Fischer S, Pomper M, Wong D,
547   Dannals R, Brust P, Horti A: **18F-JHU94620, a high affinity PET radioligand for**
548   **imaging of cannabinoid subtype 2 receptors (CB2R).** *Journal of Nuclear Medicine*
549   2015, **56:**1048-1048.
550   53. Attili B, Celen S, Ahamed M, Koole M, Haute CVD, Vanduffel W, Bormans G:
551   **Preclinical evaluation of [(18) F]MA3: a CB2 receptor agonist radiotracer for PET.**
552   *Br J Pharmacol* 2019, **176:**1481-1491.
553   54. Heimann D, Börgel F, de Vries H, Bachmann K, Rose VE, Frehland B, Schepmann D,
554   Heitman LH, Wünsch B: **Optimization of pharmacokinetic properties by**
555   **modification of a carbazole-based cannabinoid receptor subtype 2 (CB(2)) ligand.**
556   *Eur J Med Chem* 2018, **143:**1436-1447.
557   55. Kallinen A, Boyd R, Lane S, Bhalla R, Mardon K, Stimson DHR, Werry EL, Fulton R,
558   Connor M, Kassiou M: **Synthesis and in vitro evaluation of fluorine-18 benzimidazole**
559   **sulfones as CB2 PET-radioligands.** *Org Biomol Chem* 2019, **17:**5086-5098.
560   56. Haider A, Muller Herde A, Slavik R, Weber M, Mugnaini C, Ligresti A, Schibli R, Mu L,
561   Mensah Ametamey S: **Synthesis and Biological Evaluation of Thiophene-Based**
562   **Cannabinoid Receptor Type 2 Radiotracers for PET Imaging.** *Front Neurosci* 2016,
563   **10:**350.

57. Caillà F, Cacheux F, Peyronneau M-A, Jaumain E, POTTIER G, Ullmer C, Grether U, Dolle F, Damont A, Kuhnast B: **Biodistribution of [18F] FC0324, a new PET tracer targeting CB2 receptors.** *Journal of Nuclear Medicine* 2017, **58:**855-855.

58. Haider A, Gobbi L, Kretz J, Ullmer C, Brink A, Honer M, Woltering TJ, Muri D, Iding H, Bürkler M, et al: **Identification and Preclinical Development of a 2,5,6-Trisubstituted Fluorinated Pyridine Derivative as a Radioligand for the Positron Emission Tomography Imaging of Cannabinoid Type 2 Receptors.** *Journal of Medicinal Chemistry* 2020, **63:**10287-10306.

59. Haider A, Kretz J, Gobbi L, Ahmed H, Atz K, Bürkler M, Bartelmus C, Fingerle J, Guba W, Ullmer C, et al: **Structure-Activity Relationship Studies of Pyridine-Based Ligands and Identification of a Fluorinated Derivative for Positron Emission Tomography Imaging of Cannabinoid Type 2 Receptors.** *J Med Chem* 2019, **62:**11165-11181.

60. Offner H, Subramanian S, Parker SM, Afentoulis ME, Vandenbark AA, Hurn PD: **Experimental stroke induces massive, rapid activation of the peripheral immune system.** *J Cereb Blood Flow Metab* 2006, **26:**654-665.

61. Garbuzova-Davis S, Haller E, Tajiri N, Thomson A, Barretta J, Williams SN, Haim ED, Qin H, Frisina-Deyo A, Abraham JV, et al: **Blood-Spinal Cord Barrier Alterations in Subacute and Chronic Stages of a Rat Model of Focal Cerebral Ischemia.** *J Neuropathol Exp Neurol* 2016, **75:**673-688.

62. Huang B, Xie Q, Lu X, Qian T, Li S, Zhu R, Yu W, Chen G, Chen Z, Xu X, et al: **GlyT1 Inhibitor NFPS Exerts Neuroprotection via GlyR Alpha1 Subunit in the Rat Model of Transient Focal Cerebral Ischaemia and Reperfusion.** *Cell Physiol Biochem* 2016, **38:**1952-1962.

63. Dang G, Chen X, Chen Y, Zhao Y, Ouyang F, Zeng J: **Dynamic secondary degeneration in the spinal cord and ventral root after a focal cerebral infarction among hypertensive rats.** *Sci Rep* 2016, **6:**22655.

64. Moisse K, Welch I, Hill T, Volkening K, Strong MJ: **Transient middle cerebral artery occlusion induces microglial priming in the lumbar spinal cord: a novel model of neuroinflammation.** *J Neuroinflammation* 2008, **5:**29.

65. Dang G, Chen X, Zhao Y, Chen Y, Ouyang F, Liang J, Guo Y, Zeng J: **Alterations in the spinal cord and ventral root after cerebral infarction in non-human primates.** *Restor Neurol Neurosci* 2018, **36:**729-740.

66. Saleh A, Schroeter M, Jonkmanns C, Hartung HP, Mödder U, Jander S: **In vivo MRI of brain inflammation in human ischaemic stroke.** *Brain* 2004, **127:**1670-1677.

67. Ni R, Vaas M, Ren W, Klohs J: **Non-invasive detection of acute cerebral hypoxia and subsequent matrix-metalloproteinase activity in a mouse model of cerebral ischemia using multispectral-optoacoustic-tomography.** *Neurophotonics* 2018, **5:**015005.

68. Vaas M, Ni R, Rudin M, Kipar A, Klohs J: **Extracerebral Tissue Damage in the Intraluminal Filament Mouse Model of Middle Cerebral Artery Occlusion.** *Front Neurol* 2017, **8:**85.

69. Livak KJ, Schmittgen TD: **Analysis of relative gene expression data using real-time quantitative PCR and the 2(-Delta Delta C(T)) Method.** *Methods* 2001, **25:**402-408.

70. Ni R, Kindler DR, Waag R, Rouault M, Ravikumar P, Nitsch R, Rudin M, Camici GG, Liberale L, Kulic L, Klohs J: **fMRI Reveals Mitigation of Cerebrovascular**

609   **Dysfunction by Bradykinin Receptors 1 and 2 Inhibitor Noscapine in a Mouse**
610   **Model of Cerebral Amyloidosis.** *Front aging neurosci* 2019, **11:**27-27.

611 71. Ni R, Rudin M, Klohs J: **Cortical hypoperfusion and reduced cerebral metabolic rate**
612   **of oxygen in the arcAbeta mouse model of Alzheimer's disease.** *Photoacoustics* 2018,
613   **10:**38-47.

614 72. Ren W, Skulason H, Schlegel F, Rudin M, Klohs J, Ni R: **Automated registration of**
615   **magnetic resonance imaging and optoacoustic tomography data for experimental**
616   **studies.** *Neurophotonics* 2019, **6:**1-10, 10.

617 73. Vaas M, Deistung A, Reichenbach JR, Keller A, Kipar A, Klohs J: **Vascular and Tissue**
618   **Changes of Magnetic Susceptibility in the Mouse Brain After Transient Cerebral**
619   **Ischemia.** *Transl Stroke Res* 2018, **9:**426-435.

620 74. Krämer SD, Betzel T, Mu L, Haider A, Herde AM, Boninsegni AK, Keller C, Szermerski
621   M, Schibli R, Wünsch B, Ametamey SM: **Evaluation of (11)C-Me-NB1 as a Potential**
622   **PET Radioligand for Measuring GluN2B-Containing NMDA Receptors, Drug**
623   **Occupancy, and Receptor Cross Talk.** *J Nucl Med* 2018, **59:**698-703.

624 75. Lin TN, He YY, Wu G, Khan M, Hsu CY: **Effect of brain edema on infarct volume in**
625   **a focal cerebral ischemia model in rats.** *Stroke* 1993, **24:**117-121.

626 76. Ma Y, Hof PR, Grant SC, Blackband SJ, Bennett R, Slatest L, McGuigan MD,
627   Benveniste H: **A three-dimensional digital atlas database of the adult C57BL/6J**
628   **mouse brain by magnetic resonance microscopy.** *Neuroscience* 2005, **135:**1203-1215.

629 77. Pettigrew LC, Holtz ML, Craddock SD, Minger SL, Hall N, Geddes JW: **Microtubular**
630   **proteolysis in focal cerebral ischemia.** *J Cereb Blood Flow Metab* 1996, **16:**1189-1202.

631 78. Dawson DA, Hallenbeck JM: **Acute focal ischemia-induced alterations in MAP2**
632   **immunostaining: description of temporal changes and utilization as a marker for**
633   **volumetric assessment of acute brain injury.** *J Cereb Blood Flow Metab* 1996, **16:**170-
634   174.

635 79. Hosoya T, Fukumoto D, Kakiuchi T, Nishiyama S, Yamamoto S, Ohba H, Tsukada H,
636   Ueki T, Sato K, Ouchi Y: **In vivo TSPO and cannabinoid receptor type 2 availability**
637   **early in post-stroke neuroinflammation in rats: a positron emission tomography**
638   **study.** *J Neuroinflammation* 2017, **14:**69.

639 80. Vandeputte C, Casteels C, Struys T, Koole M, van Veghel D, Evens N, Gerits A,
640   Dresselaers T, Lambrichts I, Himmelreich U, et al: **Small-animal PET imaging of the**
641   **type 1 and type 2 cannabinoid receptors in a photothrombotic stroke model.** *Eur J*
642   *Nucl Med Mol Imag* 2012, **39:**1796-1806.

643 81. Jordan CJ, Xi Z-X: **Progress in brain cannabinoid CB(2) receptor research: From**
644   **genes to behavior.** *Neurosci Biobehav Rev* 2019, **98:**208-220.

645 82. Fernández-López D, Faustino J, Derugin N, Wendland M, Lizasoain I, Moro MA, Vexler
646   ZS: **Reduced infarct size and accumulation of microglia in rats treated with WIN**
647   **55,212-2 after neonatal stroke.** *Neuroscience* 2012, **207:**307-315.

648 83. Zhang M, Martin BR, Adler MW, Razdan RK, Ganea D, Tuma RF: **Modulation of the**
649   **balance between cannabinoid CB(1) and CB(2) receptor activation during cerebral**
650   **ischemic/reperfusion injury.** *Neuroscience* 2008, **152:**753-760.

651 84. Yuan H, Frank Jonathan E, Hong Y, An H, Eldeniz C, Nie J, Bunevicius A, Shen D, Lin
652   W: **Spatiotemporal Uptake Characteristics of ^{18}F-2-Fluoro-2-Deoxy-d-Glucose in**
653   **a Rat Middle Cerebral Artery Occlusion Model.** *Stroke* 2013, **44:**2292-2299.

654 85. Walberer M, Backes H, Rueger MA, Neumaier B, Endepols H, Hoehn M, Fink GR,
655   Schroeter M, Graf R: **Potential of early [(18)F]-2-fluoro-2-deoxy-D-glucose positron**
656   **emission tomography for identifying hypoperfusion and predicting fate of tissue in a**
657   **rat embolic stroke model.** *Stroke* 2012, **43:**193-198.
658 86. Jin T, Mehrens H, Wang P, Kim S-G: **Chemical exchange-sensitive spin-lock MRI of**
659   **glucose analog 3-O-methyl- d -glucose in normal and ischemic brain.** *Journal of*
660   *Cerebral Blood Flow & Metabolism* 2017, **38:**0271678X1770741.
661 87. Liu N-W, Ke C-C, Zhao Y, Chen Y-A, Chan K-C, Tan D, Lee J-S, Chen Y-Y, Hsu TW,
662   Hsieh Y-J, et al: **Evolutional Characterization of Photochemically Induced Stroke in**
663   **Rats: a Multimodality Imaging and Molecular Biological Study.** *Translational Stroke*
664   *Research* 2017, **8**.
665 88. Backes H, Walberer M, Ladwig A, Rueger MA, Neumaier B, Endepols H, Hoehn M,
666   Fink GR, Schroeter M, Graf R: **Glucose consumption of inflammatory cells masks**
667   **metabolic deficits in the brain.** *Neuroimage* 2016, **128:**54-62.
668 89. Sobrado M, Delgado M, Fernández-Valle E, García-García L, Torres M, Sánchez-Prieto J,
669   Vivancos J, Manzanares R, Moro MA, Pozo MA, Lizasoain I: **Longitudinal studies of**
670   **ischemic penumbra by using 18F-FDG PET and MRI techniques in permanent and**
671   **transient focal cerebral ischemia in rats.** *NeuroImage* 2011, **57:**45-54.
672 90. Yuan H, Frank JE, Hong Y, An H, Eldeniz C, Nie J, Bunevicius A, Shen D, Lin W:
673   **Spatiotemporal uptake characteristics of ^{18}F-2-fluoro-2-deoxy-D-glucose in a rat**
674   **middle cerebral artery occlusion model.** *Stroke* 2013, **44:**2292-2299.

675

676

677 **Figures**
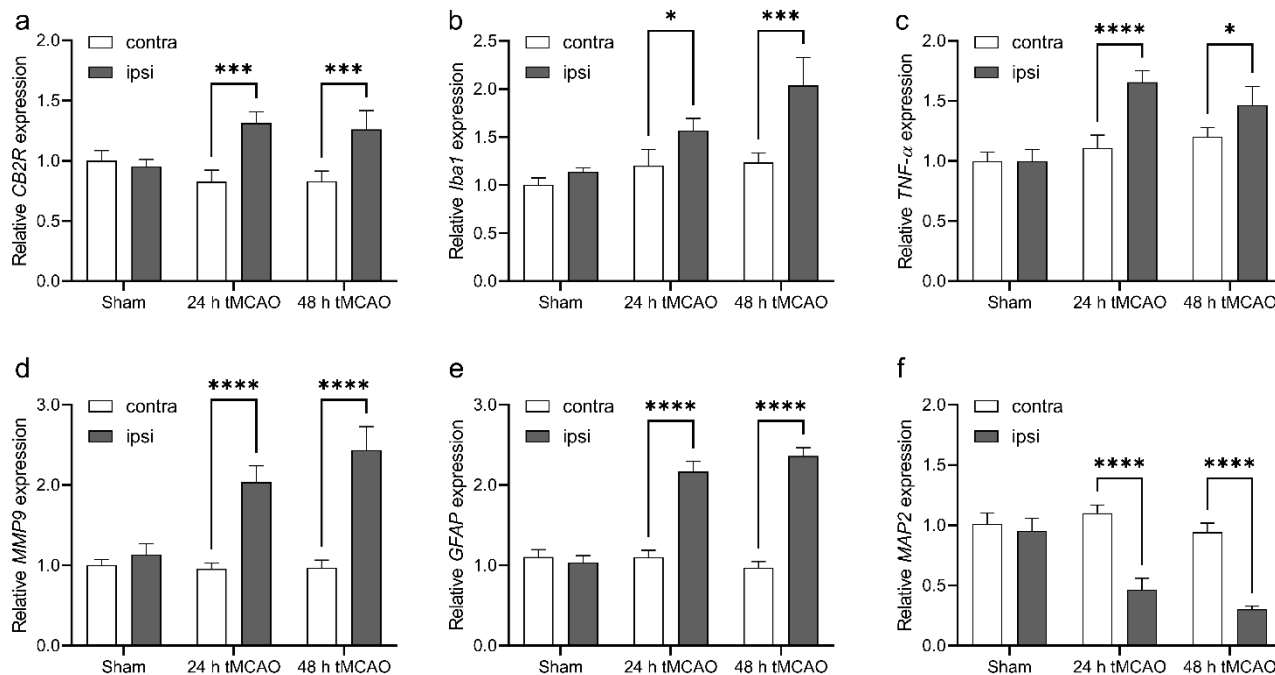
678
679 **Fig 1**. Relative mRNA levels of inflammatory markers and neuronal damage in sham-operated

680 and tMCAO mouse brain in contra-and ipsilateral brain hemisphere at 24 h and 48 h after

681 reperfusion. (a) *CNR2, (b) Iba1, (c) TNF-α, (d) MMP9, (e) GFAP* and (f) *MAP-2* . Values

682 represent mean ± standard deviation. Expression levels were quantified by qPCR relative to β-

683 actin.

684
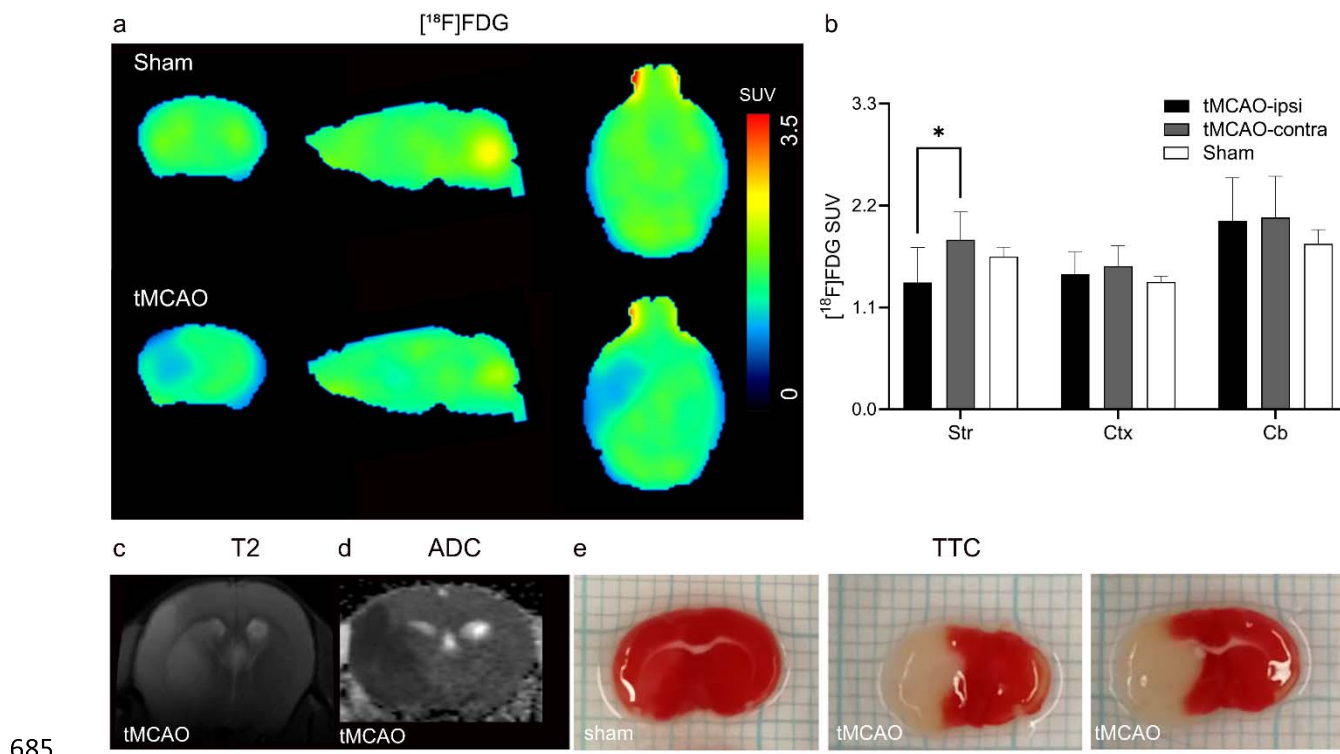
Fig 2. *In vivo* MRI and [^{18}F]FDG PET in tMCAO mouse brain. (**a**) Representative PET images of coronal, sagittal and horizontal mouse brain sections after intravenous injection of [^{18}F]FDG in sham-operated and tMCAO mice. The radiosignals were averaged from 21-61 min; (**b**) [^{18}F]FDG accumulation (SUV) at different mouse brain regions (Str: striatum; Ctx: cortex; Cb: cerebellum) in sham and tMCAO mice. Significantly reduced [^{18}F]FDG accumulation was observed in the ipsilateral striatum compared to contralateral side in tMCAO mice; (**c-e**) *In vivo* T$_2$-weighted image, ADC map and *ex vivo* TTC stained brain sections, indicating the delineation in tMCAO mice. TTC: 2,3,5-triphenyltetrazolium chloride; ADC: apparent diffusion coefficient; SUV: standard uptake value.
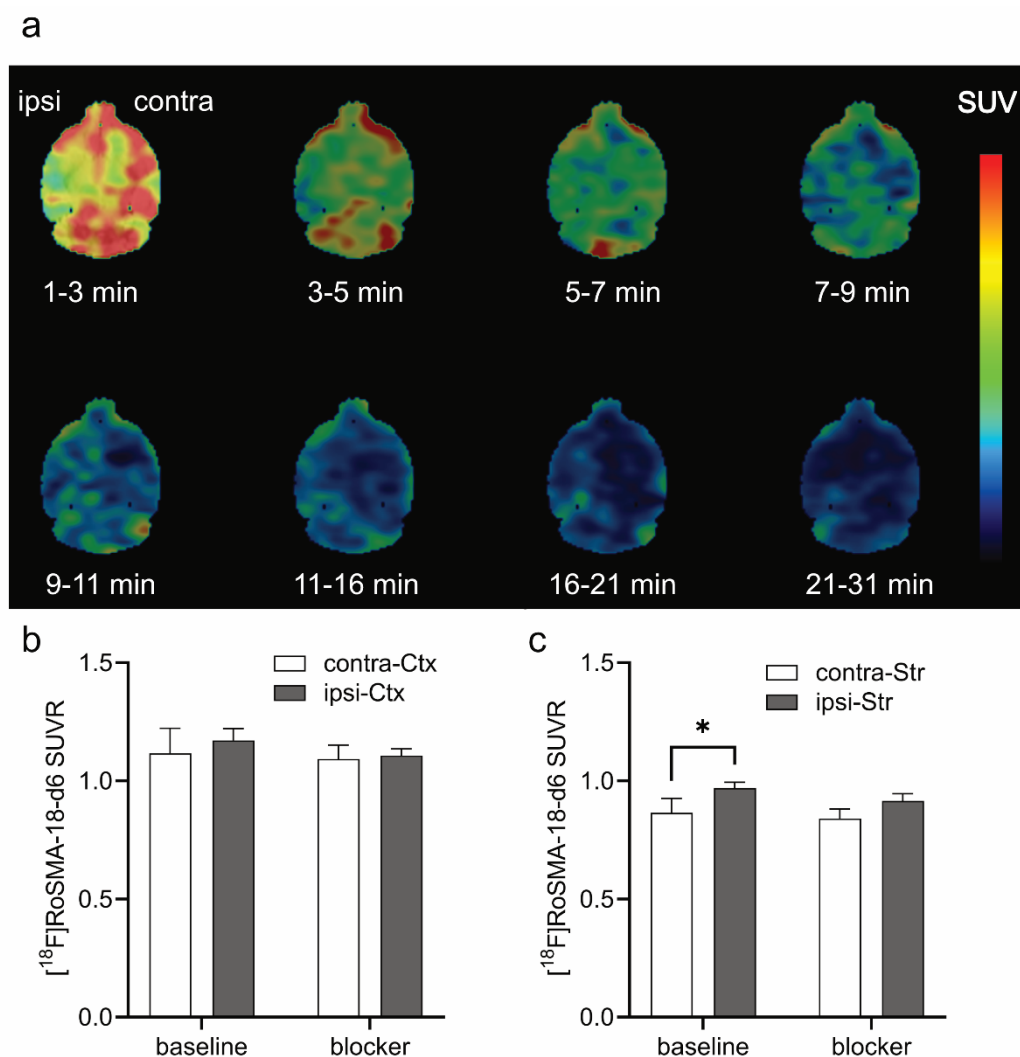
27

Fig 3. *In vivo* microPET imaging of tMCAO mouse brain using [18F]RoSMA-18-d6. (**a**) Representative PET images of horizontal mouse brain sections at different time frames after intravenous injection of [18F]RoSMA-18-d6; SUV: 0-0.5; (**b, c**) Ratios of [18F]RoSMA-18-d6 uptake under baseline and blockade conditions in cortex and striatum. Significantly higher [18F]RoSMA-18-d6 standard uptake value ratio (SUVR) was observed in the ischemic ipsilateral striatum under baseline conditions, but not in the ipsilateral cortex. Midbrain was used as reference brain region for SUVR calculation.

28
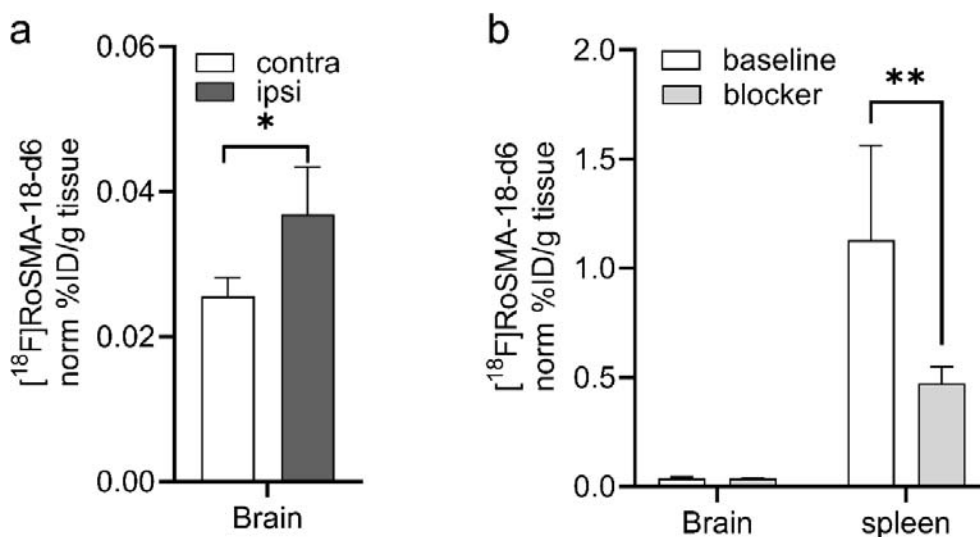
Fig 4. *Ex-vivo* biodistribution of [18F]RoSMA-18-d6 in the brain and spleen of tMCAO mouse. Animals (n=4) were sacrificed at 70 min post-injection, the spleen and brain regions were dissected and analyzed with a gamma counter. (**a**) Higher [18F]RoSMA-18-d6 binding (norm% ID/g tissue) was detected in the ipsilateral vs contralateral hemisphere under baseline conditions. (**b**) In the spleen about 58 % of the [18F]RoSMA-18-d6 binding (norm% ID/g tissue) was blocked. No significant blocking was observed in the brain. Data are presented as the mean of the percentage of injected dose per gram tissue normalized to 20 g body weight; mean ± standard deviation. % ID/g: percentage injected dose per gram.

719 **Additional files:**

720 Additional file 1: Supplementary Figure 1. Time activity curves of [^{18}F]RoSMA-18-d6 *in vivo*

721 microPET imaging of tMCAO mouse brain. (**a-d**) In the cortex, striatum, cerebellum and

722 midbrain under baseline and blockade conditions. No difference in [^{18}F]RoSMA-18-d6 SUV was

723 observed in different brain regions at ipsilateral vs contralateral side under baseline or blockade

724 conditions. Data represent mean ± standard deviation.

725

726 Additional file 2: Supplementary Table 1. Primers used for the quantitative polymerase chain

727 reaction assay on mouse brain tissue

728